Ana M. Martins, Rafeeq Tanbour, Mohammed A. Elkhodiry and Ghaleb A. Husseini*

Ultrasound-induced doxorubicin release from folate-targeted and non-targeted P105 micelles: a modeling study

DOI 10.1515/ejnm-2015-0045
Received November 11, 2015; accepted January 5, 2016

Abstract: The aim of this work is to study the kinetics of ultrasound (70 kHz) – using a kinetic model that takes into account cavitation events and drug re-encapsulation upon the cessation of the acoustic field. The simulation allowed the determination of three parameters α, β and λ that define the release and re-encapsulation behavior of this drug delivery system (DDS). The results showed that the drug release increased with increasing power density, as evidenced by the correlation between α and power density. The micelle re-assembly, quantified by the parameter β, also increased with increasing power density. The parameter λ, which is associated with the initial phase of the release process, showed a constant value regardless of the power density. The significance of these results was discussed. Additionally, a comparison between these parameters in folate-targeted and non-targeted micelles showed statistically significant differences for several power densities examined. A better understanding of the kinetics involved in this DDS is very important for the determination of the optimum ultrasound parameters to be used in future in vitro and in vivo experiments.

Keywords: cavitation; Dox; folic acid; micelles; Pluronic® P105; ultrasound.

Introduction

Cancer is the leading cause of death in Europe and North America, and the second leading cause of death in the less developed countries, especially in Africa (1, 2). Cancer treatment usually involves surgery, chemotherapy, radiotherapy or, more often, a combination of these. The high toxicity of chemotherapeutic drugs limits their use, as they do not discriminate between healthy and cancerous cells. This is detrimental for healthy cells and organs, leading to the common side effects experienced by patients undergoing chemotherapy, including hair loss, nausea, fatigue, diarrhea, pain, and others. A way to overcome the unwanted side effects mentioned above is to design strategies to increase the drug delivered to cancer cells, while minimizing its concentration in healthy tissues and organs (3, 4). This involves controlling the drug delivery in space and time, and can be achieved using a nanocarrier to encapsulate the drug, and an internal or external stimulus to trigger the release of the therapeutic agent (3–5).

There are many types of nanocarriers that can be used to design drug delivery systems (DDS), including liposomes, micelles, nanospheres, nanocapsules, dendrimers, solid lipid nanoparticles and others (6).

The nanoparticles used in this work were polymeric micelles, which are colloidal particles with a diameter of 5–100 nm, composed of amphiphilic block copolymers that self-assemble in aqueous solutions, when the concentration is above the critical micellar concentration (CMC) (7). The structure formed has a semi-solid hydrophobic core, which can trap the drug, and a hydrophilic corona which establishes hydrogen bonds with water molecules, thus stabilizing the micelles (7, 8). This corona also reduces the in vivo particle recognition by opsonin proteins, hence it protects the micelles from the phagocytic clearance by the reticuloendothelial system (RES) (9).

The most widely researched polymeric micelles in acoustically activated drug delivery are triblock copolymers of poly(ethylene oxide) (PEO) and poly(propylene oxide) (PPO), commercially available as Pluronic® (10). One of the most studied Pluronic® compounds is P105 (11–13). This copolymer has a $(PPO)_{56}$-$(PEO)_{37}$-$(PPO)_{56}$ structure, with an average molecular weight of 6500, and a CMC of approximately 1 wt% at room temperature (14). The micelles have a hydrodynamic radius between 5 and 20 nm (15). Pluronic® P105 micelles have a core-shell structure, with a core formed by the hydrophobic PPO, while the hydrophilic PEO chains form the corona (Figure 1) (16).

***Corresponding author: Ghaleb A. Husseini,** Department of Chemical Engineering, American University of Sharjah, PO Box 26666, Sharjah, UAE, Phone: +971-6-515 2970, Fax: +971-6-515 2979, E-mail: ghusseini@aus.edu
Ana M. Martins, Rafeeq Tanbour and Mohammed A. Elkhodiry: Department of Chemical Engineering, American University of Sharjah, Sharjah, UAE

https://doi.org/10.1515/ejnm-2015-0045

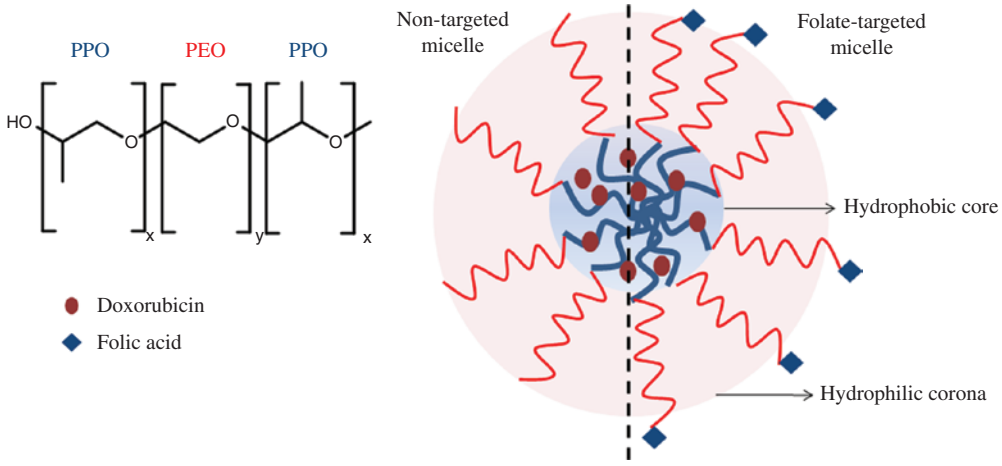

Figure 1: Schematic structure of the non-targeted and folate-targeted Pluronic® P105 micelles.

Polymeric micelles have several advantages as drug nanocarriers: (i) their CMC is very low, hence they remain stable at very low polymer concentrations (17); (ii) they have longer blood circulation times, which increases the drug bioavailability; (iii) their small size allows their preferential accumulation at the tumor site through the enhanced permeability and retention effect (EPR), also called passive targeting, by which nanoparticles preferentially extravasate at angiogenic tumor vessels (18); additionally, their size allows them to evade renal excretion (8); (iv) they can carry poorly soluble drugs (e.g. doxorubicin, Dox, commonly used in chemotherapy) in their cores which if administered in a free form, (8); (v) the use of ultrasound can destabilize the micelles, allowing the drug to be released, but the drug is re-encapsulated when insonation ceases (19); (vi) Pluronic® copolymers can sensitize multi-drug resistance (MDR) cancer cells to increase the cytotoxicity of several anticancer drugs, including Dox (20); (vii) micelles with cross-linked cores can be designed to have longer half-lives and stability [e.g. see (21)]; (viii) they have a prolonged shelf-life (19).

Despite all these advantages, there are still some challenges with the use of micelles as DDS, such as their small size which limits the amount of drug they can encapsulate (22). Increasing the size of the micelles decreases their stability and promotes aggregation.

Drug delivery systems using micelles can be modified to have an increased antitumor efficacy. Several methods have been explored to increase the accumulation of the micelles at the tumor site, and then trigger the release of their contents in a controlled manner. Hence, multifunctional micelles have been designed, being used to achieve active and/or triggered targeting (23, 24).

In active targeting, the surface of the nanoparticle is modified with a moiety that allows their specific binding to receptors overexpressed in cancer cells (25). Hence, there is an increased accumulation of the nanoparticles at the tumor site and an increased uptake via receptor-mediated endocytosis (26). One of the most widely used ligands in active targeting is folic acid. Folic acid is vitamin B9, a molecule essential for several processes including cell growth and division, hence a folate receptor is highly overexpressed in several tumor cells, such as in ovarian, brain, breast and lung cancer (27–31). Yoo and co-workers (32) synthesized Dox-encapsulating poly(D,L-lactic-*co*-glycolic acid) (PLGA) – poly(ethylene glycol) (PEG) micelles conjugated to folate, and studied their effect on human KB carcinoma cells. Flow cytometry and confocal microscopy showed that the cellular uptake of the targeted micelles was much higher than that of unconjugated micelles, and that the cytotoxicity of these micelles was higher than that of free Dox. In vivo studies using a nude mice model showed that the systemic administration of these micelles significantly regressed tumor growth, due to their accumulation in the tumor tissue. Hayama et al. (33) prepared camptothecin-loaded polymeric micelles modified with folate moieties and studied the carriers' uptake by KB cells (overexpressing the folate receptor FR+) and in HepG2 cells (folate-negative control cells FR-), using flow cytometry, fluorescence microscopy and confocal laser scanning microscopy. The results showed an increased uptake and increased cytotoxicity in the case of KB cells, but not in the HepG2 cells.

To further increase the specificity of the chemotherapy, it is desirable to control the release of the drug, encapsulated in polymeric micelles or other nanoparticles, when these reach the tumor site. This is called triggered or actuated

targeting, and it uses stimuli, such as temperature increase, magnetic or electric fields, pH changes, ultrasound exposure, to induce the release of the drug from the nanocarrier (9). The use of ultrasound to trigger the drug release from polymeric micelles has been widely researched (15, 16, 19, 34). Husseini et al. (35) used folate-targeted Pluronic® P105 micelles to study the US-induced release using 70-kHz US at several power densities. The results showed that above a threshold of 0.55 W/cm^2, Dox is released from the micelles, and this release increases with increasing power density (up to 5.4 W/cm^2). Kim et al. (36) also reported a study of triggered targeting using pH-sensitive micelles of poly(L-histidine-*co*-L-phenylalanine)-*b*-PEG-folate. Their in vivo study used MDR ovarian-tumor (A2780/Dox^R)-xenografted mouse models and studied the extravasation and drug biodistribution as a function of time, using noninvasive imaging techniques. Results showed that the drug accumulated in the tumor during the first hour post-injection, that the micelles had a longer circulation time, and evidenced the intracellular drug delivery. Additionally, the authors reported a suppression of the tumor growth in animals treated with this micellar formulation.

In this paper, we implemented a previously described kinetic model of the Dox release and subsequent re-encapsulation from polymeric Pluronic® P105 micelles (37, 38) in MATLAB (MathWorks, Natick, MA, USA), and used it to fit experimental data obtained in vitro. The data concerns the application of 70-kHz US, at different power densities, to Dox-containing micelles, either non-targeted (P105) (37), or folate-targeted (F-P105) (35). This allowed the calculation of rate constants related to Dox release and re-encapsulation, and the investigation of how these change with power density. A comparison between P105 and F-P105 was also performed, and the results discussed.

Methodology

Model description

The model used in this work was originally used to calculate the kinetic parameters associated with the release and re-encapsulation phenomena associated with drug delivery systems (DDS), as described in (37) and (38). The main concept behind this model is the cavitation phenomenon that generates shock waves piercing/shearing the micelles open and releasing the drug (38).

The first paper (38) proposes simultaneous mechanisms for the process of drug release, and it assumes the mechanism to be first order. The mathematical summary of this physical mechanism is given below.

(1) The micelles used were Pluronic® P105 with a diameter ranging between 10 and 20 nm. The micelles were divided into five groups based on their diameter, with each group containing 20% of the polymer. The fraction of the total number of micelles which were initially in each group ($M_{j,o}$) can be calculated using equation [1]:

$$M_{j,o}=\frac{(\text{volume of polymer}/\text{volume of one micelle})_j}{\sum_{i=1}^{n}(\text{volume of polymer}/\text{volume of one micelle})_i} \quad [1]$$

(2) The number of micelles in each group changed with time due to two competing mechanisms: (i) the destruction of the micelles during insonation, and (ii) their reassembly. The change in the number of micelles with time is given by the equation:

$$\frac{dM_j}{dt}=\left(\frac{dM_j}{dt}\right)_{\text{destruction}}+\left(\frac{dM_j}{dt}\right)_{\text{assembly}} \quad [2]$$

(a) The rate of micelle destruction is given as follows:

$$\left(\frac{dM_j}{dt}\right)_{\text{destruction}}=-k_{d,j}M_jN \quad [3]$$

where, $k_{d,j}$ is the rate constant which depends on the size of the micelles, with the following proportional relationship with the micelle diameter, $\overline{D}_j$:

$$k_{d,j}=\alpha\frac{\overline{D_j}}{N_0} \quad [4]$$

where α is a non-zero constant during insonation, turning to zero when the insonation period was over, and N_0 is the initial number of cavitating nuclei.

N is the number of cavitating nuclei, and its value is assumed to decrease slowly with time because of bubble collapsing which happens at all power densities used to collect the release data. The rate of this decrease is given by:

$$\frac{dN}{dt}=-k_NN \quad [5]$$

If equation [5] is integrated, the resulting solution is:

$$N=N_0\exp(-k_Nt) \quad [6]$$

The rate of micelle reassembly is given as follows:

$$\left(\frac{dM_j}{dt}\right)_{\text{assembly}}=k_{a,j}V_{FP} \quad [7]$$

$k_{a,j}$ is a rate constant that depends on the size of the formed micelles. The formation here depends on the polymer volume, so the constant is proportional to the inverse of the diameter cubed:

$$k_{a,j}=\frac{\beta}{(\overline{D_j^3})} \quad [8]$$

V_{FP} is the normalized volume concentration. It is obtained by dividing the volume of free polymer in the solution, v_{FP} by the volume of the solution, v_{sol}; then normalizing this value by the concentration that would occur if the polymeric chains were freely available in the solution $v_{\text{tot},o}/v_{\text{sol}}$:

$$V_{FP}=\frac{v_{FP}/v_{\text{sol}}}{v_{\text{tot},o}/v_{\text{sol}}}=\frac{v_{FP}}{v_{\text{sol}}} \quad [9]$$

The volume of free polymer v_{FP} is equal to the initial total volume of polymer in the solution minus the volume of polymer in all the micelles at a certain time, then:

$$V_{FP}=1-\frac{v_{\text{tot}}}{v_{\text{tot},o}} \quad [10]$$

To relate the total volume to the volumes of all micellar groups:

$$V_{FP}=1-\frac{\sum_{j=1}^{n} M_j(\pi/6)\overline{D_j^3}}{\sum_{j=1}^{n} M_{j,o}(\pi/6)\overline{D_j^3}} \quad [11]$$

Since $M_{j,o}$ is the initial fraction of micelles in group j, which equals $1/n$, hence:

$$V_{FP}=1-n\frac{\sum_{j=1}^{n} M_j D_j^3}{\sum_{j=1}^{n} D_j^3} \quad [12]$$

(3) The amount of drug encapsulated changes with time due to two mechanisms: the first is the release of the drug into solution, after the destruction of micelles, while the second is the re-encapsulation of the drug inside the micelles:

$$\frac{dE_j}{dt}=\left(\frac{dE_j}{dt}\right)_{\text{destruction}}+\left(\frac{dE_j}{dt}\right)_{\text{encapsulation}} \quad [13]$$

(a) The rate of drug release is related to the destruction of micelles. The drug concentration is assumed to be the average of the drug concentration within its corresponding group, E_j/M_j:

$$\left(\frac{dE_j}{dt}\right)_{\text{destruction}}=\left(\frac{dM_j}{dt}\right)_{\text{destruction}}\left(\frac{E_j}{M_j}\right) \quad [14]$$

Using Eq. [3]:

$$\left(\frac{dE_j}{dt}\right)_{\text{destruction}}=-k_{d,j}NE_j \quad [15]$$

(b) After micellar reassembly, the free drug is re-encapsulated. The amount of free drug, F, depends on the capacity of the newly formed micelles. This capacity is the difference between saturation (if the whole capacity is filled) and the actual amount,

$$\left(\frac{dE_j}{dt}\right)_{\text{encapsulation}}=k_{e,j}F(E_j^{\text{sat}}-E_j) \quad [16]$$

where $K_{e,j}$ is a rate constant which depends on the ratio of the surface area to the volume, so it is inversely proportional to the micellar mean diameter:

$$k_{e,j}=\frac{\gamma}{(\overline{D_j})} \quad [17]$$

The saturation concentration of the drug that can be encapsulated inside the micelles depends on the number of micelles in each group, the volume of each micelle and the amount of drug that can be stored per unit volume, $\rho_{\text{Dox}}^{\text{sat}}$:

$$E_j^{\text{sat}}=M_j\frac{\pi}{6}\overline{D_j^3}\rho_{\text{Dox}}^{\text{sat}} \quad [18]$$

$\rho_{\text{Dox}}^{\text{sat}}$ can be considered as the total amount of drug that can be encapsulated in an initial total volume within the micelles:

$$E_j^{\text{sat}}=M_j\frac{\pi}{6}\overline{D_j^3}\frac{E_{\text{tot},o}^{\text{sat}}}{v_{\text{tot},o}} \quad [19]$$

The total initial volume $v_{\text{tot},o}$ can be related to the sum of the initial volumes of all micellar groups:

$$E_j^{\text{sat}}=nM_j\frac{\overline{D_j^3}}{\sum_{j=1}^{n}\overline{D_j^3}}E_{\text{tot},o}^{\text{sat}} \quad [20]$$

The total amount of the drug is the sum of the free fraction and the encapsulated fraction, hence the free amount of the drug in the solution, F, is:

$$F=1-E \quad [21]$$

The amount of encapsulated drug, E is the sum of the fraction of encapsulated drug in each group:

$$E=\sum_{j=1}^{n}E_j \quad [22]$$

In (37), a simplification of the encapsulation model (Eq. [16]) was described. It was assumed that the saturation amount of drug, E_j^{sat} is very large compared with the encapsulated drug amount in group j, E_j. So it was assumed that E_j is negligible, and equation [16] was simplified to:

$$\left(\frac{dE_j}{dt}\right)_{\text{encapsulation}}=k_{e,j}FE_j^{\text{sat}} \quad [23]$$

Then by substituting all the terms from the previous equations, we obtained:

$$\left(\frac{dE_j}{dt}\right)_{\text{encapsulation}}=\frac{\gamma}{(\overline{D_j})}FnM_j\frac{\overline{D_j^3}}{\sum_{j=1}^{n}\overline{D_j^3}}E_{\text{tot},o}^{\text{sat}} \quad [24]$$

The three constants γ, n, $E_{\text{tot},o}^{\text{sat}}$ can be incorporated in one single term; the encapsulation parameter, λ:

$$\left(\frac{dE_j}{dt}\right)_{\text{encapsulation}}=\boldsymbol{\lambda}FM_j\frac{\overline{D_j^3}}{\overline{D_j}\sum_{j=1}^{n}\overline{D_j^3}} \quad [25]$$

The model was implemented in MATLAB and used to calculate all the parameters related to release, re-encapsulation and reassembly, namely $\boldsymbol{\alpha}$, $\boldsymbol{k_n}$, $\boldsymbol{\beta}$ and $\boldsymbol{\lambda}$. These four kinetic parameters were compared for the acoustic release of Dox from folated versus non-folated micelles. The results obtained were also used to determine if these kinetic rates are a function of power intensity.

Experimental data collection

The experimental data used for the modeling process described in this work were obtained by Husseini et al., for folated micelles (35) and non-targeted micelles (37). In both cases, the micelles used were Pluronic® P105 encapsulating Dox. Ultrasonication was performed at 70 kHz, using a sonicator bath (Sonicor 100, Copiague, NY, USA) at 37°C.

The P105 micelles were prepared by dissolving Pluronic® P105 (BASF Corporation, Mount Olive, NJ, USA) in phosphate buffered saline, while the folate (Sigma-Aldrich, St. Louis, MO, USA) moiety

was attached as described in (35). Dox (obtained in a 1:5 mixture with lactose from Pharmacia & Upjohn Company, Kalamazoo, MI, USA) was encapsulated in the micelles by mixing at room temperature, to a final concentration of 10 μg/mL.

A custom ultrasonication chamber was designed by the same group (39) to measure the fluorescence changes caused by the Dox release in the presence of US. The micellar samples were inserted in cuvettes and the fluorescence emissions were measured upon excitation at 488 nm. As Dox exhibits a large decrease in fluorescence when transferred from the micelle hydrophobic core to the aqueous buffer solution (phosphate buffered saline, PBS), the release can be followed by monitoring this decrease in the presence of US. For this purpose, the sonication chamber was attached to a fluorescence detector that continuously monitored the fluorescence level of the sample. Before sonication, the fluorescence level was measured for a 10 s period, which corresponds to a 100% encapsulation level (I_{P105}). At the 10 s mark, the US was turned on leading to the release of some of the encapsulated drug. The fluorescence level at this instant (I_{US}) was <100% – our experimental set-up was measuring the percentage of encapsulated drug. After 10 s of insonation, the US was turned off and the fluorescence level was monitored for another 10 s, leading to a total measurement time of 30 s. The measurements of the fluorescence level were collected using a computer software that controlled the detector. The fraction of encapsulated Dox, E, was calculated using Eq. [26]:

$$E=\frac{I_{US}-I_{PBS}}{I_{P105}-I_{PBS}} \quad [26]$$

where I_{PBS} is the baseline fluorescence of Dox in PBS, in the absence of micelles (corresponds to 100% release).

Data Analysis

Data denoising and preparation: The first step in data analysis was the pre-processing of the raw experimental data, as it contains high levels of noise. The data were pre-processed as follows:

Data overlaying

As the US was manually turned on and off, the experimental results needed to be superimposed to make the on and off time points coincide. This was done by excluding some of the initial data collected before the US was turned on. Afterwards a 5-point average was applied in order to reduce the noise. The wavelet denoising algorithm and the 5-point moving average were used to smooth the data and get a reasonable fit to our model.

Data Denoising

The noise was reduced using the wave menu property in the MATLAB software. This property is based on the wavelet concept which is robust in denoising data. In MATLAB software, the command wavmenu opens a GUI that allows the user to perform dynamic denoising by changing the parameters manually while observing the output continuously. This procedure was repeated for all runs. The graph was then divided into two parts: the release and the re-encapsulation parts, as shown in Figure 2.

Data modeling using the MATLAB designed program: The model described previously is the basis of this study, and data modeling

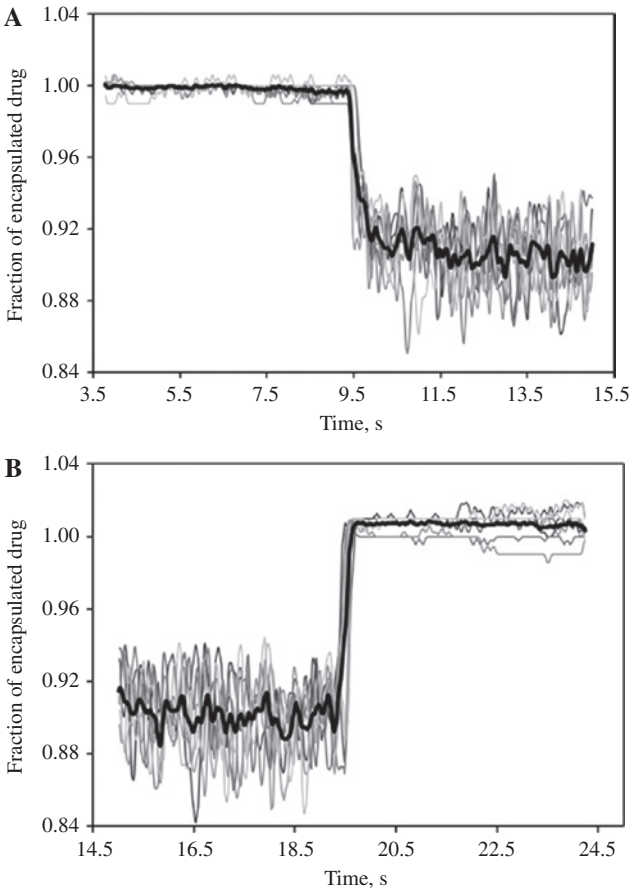

Figure 2: Averaging of the data (black bold lines) showing the temporal release for one of the micelle samples. (A) Release part, (B) re-encapsulation part. The figure shows nine replicates of a F-P105 sample, as an example.

was used to calculate the kinetic parameters involved in the acoustically activated release of Dox from Pluronic® micelles and subsequent re-encapsulation. The steps for the work were as follows:

(a) The model equations were rearranged as the two following equations:

$$\frac{dM_j}{dt}=\left[-(\alpha\overline{D_j})M_j(\exp(-k_N t))\right]+\left[\left(\frac{\beta}{(D_j^3)}\right)\left(1-n\frac{\sum_{j=1}^{n}M_jD_j^3}{\sum_{j=1}^{n}D_j^3}\right)\right] \quad [27]$$

$$\frac{dE_j}{dt}=\left[-(\alpha\overline{D_j})(\exp(-k_N t))E_j\right]+\left[\lambda FM_j\frac{\overline{D_j^3}}{\overline{D_j}\sum_{j=1}^{n}\overline{D_j^3}}\right] \quad [28]$$

In these equations, there are four parameters α, β, λ and k_N that need to be determined. The parameter k_N, which is related to the number of cavitating nuclei, is assumed to be zero in the data collected. This parameter is calculated from the upward slope of the partial recovery phase. In the data used, the recovery phase is almost linear, hence k_N was assumed to be negligible. The other three parameters have to be determined simultaneously, as described above. The modeling process at hand cannot be done analytically, as there are two equations with three

unknowns, so numerical methods were used to represent the kinetics of the system.

(b) In order to determine these parameters numerically, the MATLAB program was designed, based on the least squares method. The code contains two files: the function file, and the script file. In the function file, the main equations used were defined along with their derivatives and the output was returned to the script file to be used in the least squares equation. The derivatives of these equations were calculated numerically using the finite difference forward formulas and a time step of 0.02 s. As an example, the derivatives *dM* and *dE* were found as follows:

$$dM_{j(i)} = \frac{M_{j(i+1)} - M_{j(i)}}{dt} \quad [29]$$

$$dE_{j(i)} = \frac{E_{j(i+1)} - E_{j(i)}}{dt} \quad [30]$$

The least squares method compares experimental data with the given model, and provides the best fit. The experimental data for our work are the percentage of drug release (*E*) for two different micelles, folated micelles (F-P105) and non-folated micelles (P105). The initial values for the drug amount (*Ej*) were assumed to be the same for the five proposed groups of micelles: 0.2 for each group. The initial values for the model parameters reported by Stevenson-Abouelnasr et al. (38).

In the function file, the two main equations described earlier were adapted for each of the five groups of micelles, i.e. ten equations were entered, five for (*M*) and five for (*E*). The least squares method code was used with given upper and lower limits within which the result should fall.

(c) The code was then executed using the data collected at the moment the US was turned on, until the point after the partial recovery phase such that the entire release profile was considered, as shown in Figure 3.

(d) After exporting the data, the start and end points, as well as entering the data length for every run, the code was executed. The resultant plot compares the fraction encapsulated vs. time of the experimental data with the kinetic model described above, and generates the values for the parameters. An example of the results is shown in Figure 4.

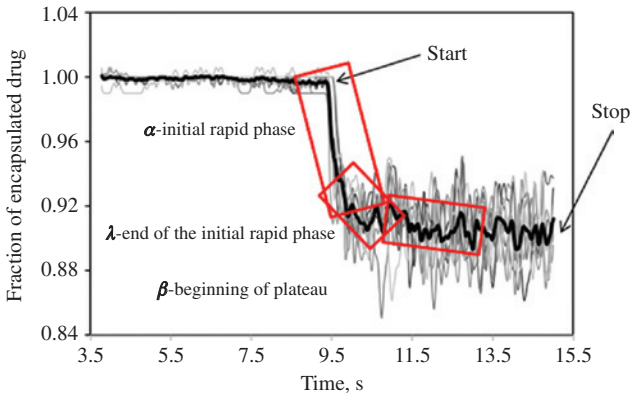

Figure 3: Start and stop points for the modeling. The figure shows the phases of the curve used for the determination of the three model parameters α, β and λ.

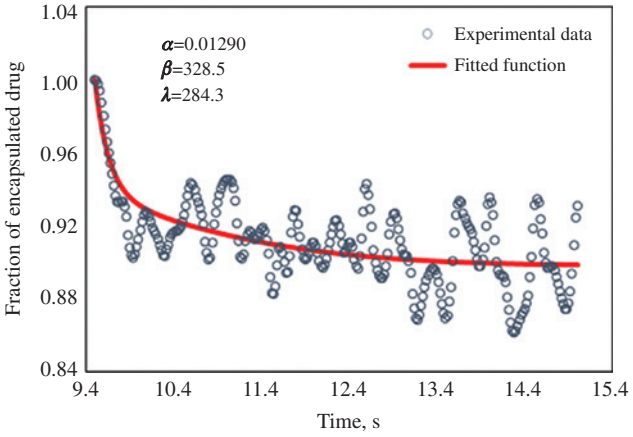

Figure 4: Example of a modeling result using the MATLAB program.

Statistical analysis: The Tukey method is a statistical multiple comparison test used to determine if individual means are significantly different from a set of means (40). The test makes use of the average of each set of data, calculates the difference between any pair of these averages, and compares it to the standard error. If the difference is less than the standard error, the means are assumed to have no statistically significant difference; otherwise, the means are considered statistically significantly different. For unequal sample sizes, a modification of this method, introduced by Clyde Kramer in 1956 (41), can be used, and the test is referred to as the Tukey-Kramer test. In this work, the Tukey-Kramer test (with 95% confidence) was performed for the means of every parameter obtained for every power density studied, to investigate if the results were significant (i.e. if α, β, and λ significantly changed with increasing power densities).

To assess the significance of the differences between folated and non-folated micelles, for α, β, and λ, a t-test was performed, using a cutoff value of $p<0.05$.

Results and discussion

Modeling studies are extremely important in a research strategy. Models integrate and interpret data, and allow in silico predictions, guiding the design of new wet lab experiments.

In this study, experimental data concerning the kinetics of Dox release and re-encapsulation in folate-targeted (35) and non-targeted (37) P105 polymeric micelles, were used to study four parameters related to this process. As one of them, k_N, was assumed to be zero, the other three were estimated by a regression model. We then studied how each changed with increasing US power densities (Figures 5–7, Tables 1–6), followed by a comparison of the results obtained for targeted and untargeted micelles (Figures 5–7, Table 7). The power density used in the experiments was changed by varying the voltage input of the US transducer. Then the voltage values were converted

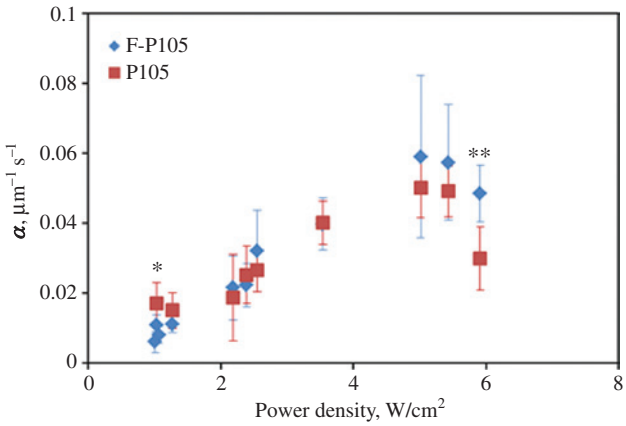

Figure 5: The relation between the parameter α and the ultrasound power density, for folated and non-folated P105 micelles. Alpha is a measure of the micellar destruction induced by ultrasound. *Power densities for which α_{P105} is significantly higher ($p<0.05$) than $\alpha_{F\text{-}P105}$; **Power densities for which α_{P105} is significantly lower ($p<0.05$) than $\alpha_{F\text{-}P105}$.

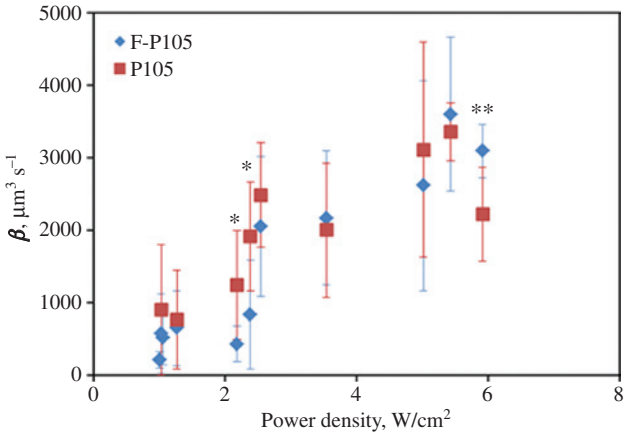

Figure 6: The relation between the parameter β and the ultrasound power density, for folated and non-folated P105 micelles. Beta is related to the micellar re-assembly rate. *Power densities for which β_{P105} is significantly higher ($p<0.05$) than $\beta_{F\text{-}P105}$; **power densities for which β_{P105} is significantly lower ($p<0.05$) than $\beta_{F\text{-}P105}$.

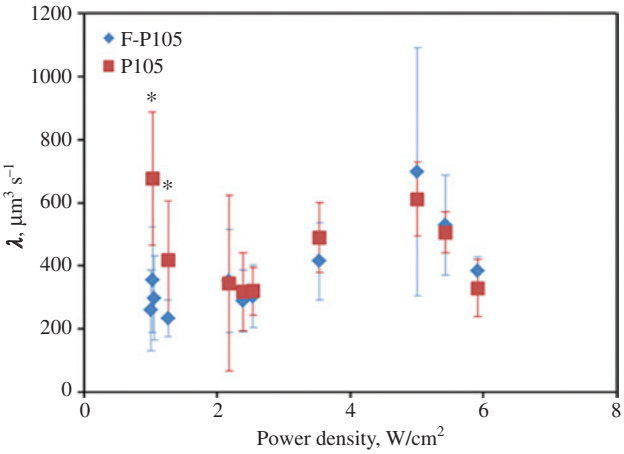

Figure 7: The relation between the parameter λ and the ultrasound power density, for folated and non-folated P105 micelles. Lambda is related to the drug re-encapsulation when ultrasonication ceases. *Power densities for which λ_{P105} is significantly higher ($p<0.05$) than $\lambda_{F\text{-}P105}$.

to power densities, as shown in Table S1 (Supplementary Data). Studying the variability in release between power densities and between the targeted and non-targeted micelles offers the information needed to optimize an ultrasound induced micellar DDS in future in vivo studies.

To investigate if α, β, and λ significantly change with increasing power densities, the Tukey-Kramer test (with 95% confidence) was performed for the means of every parameter obtained at each power density. The results are summarized in Tables 1–6. The upper part of these tables indicates the minimum significant difference (standard error), while the bottom part shows the results for the actual difference between each set of data. Significantly different results are shown in bold. To investigate if the results are significantly different for targeted vs. non-targeted micelles a t-test was performed and the results are presented in Table 7.

Alpha (α)

Alpha is a destruction parameter which represents how micelles are quickly destroyed upon insonation (38). Based on the equation of micelles ($\frac{dM}{dt}$), as α increases, the amount of micelles (M) decreases, proving the concept that after insonation starts, micelles are rapidly destroyed due to cavitation. Alpha depends on temperature, the diameter of the micelles and increases with increasing power densities, as reported by Husseini et al. (37) for non-targeted P105 micelles.

The results obtained for α, for both folated and non-folated micelles, are presented in Table S2 (Supplementary Data), and were plotted in the graph shown in Figure 5, where results are the average±standard deviation of the replicate number indicated in Table S1 (Supplementary data). For both types of micelles, a clear positive relationship exists between α and the power density. The Tukey-Kramer test results show that only about 50% of the data are significant, emphasizing that the significant differences are between the lowest (<2 W/cm²) and highest (>2 W/cm²) power densities (Tables 1 and 2). The release is assumed to be the result of cavitation, however, at higher power densities, other parameters such as the local/

Table 1: Tukey-Kramer test results for the parameter α in F-P105 micelles.

Power density, W/cm²	1.009	1.062	1.030	1.267	2.183	2.389	2.546	3.540	5.013	5.432	5.914
1.009	–	0.0153	0.0169	0.0221	0.0191	0.0169	0.0175	0.0175	0.0182	0.0169	0.0247
1.062	0.0089	–	0.0166	0.0219	0.0189	0.0166	0.0172	0.0172	0.0179	0.0166	0.0245
1.030	0.0105	0.0016	–	0.0230	0.0202	0.0180	0.0186	0.0186	0.0193	0.0180	0.0255
1.267	0.0088	0.0177	0.0193	–	0.0247	0.0230	0.0234	0.0234	0.0240	0.0230	0.0292
2.183	0.0165	**0.0254**	**0.0271**	0.0077	–	0.0202	0.0207	0.0207	0.0213	0.0202	0.0271
2.389	**0.0262**	**0.0351**	**0.0368**	0.0174	0.0097	–	0.0186	0.0186	0.0193	0.0180	0.0255
2.546	**0.0270**	**0.0359**	**0.0375**	0.0182	0.0105	0.0008	–	0.0191	0.0198	0.0186	0.0259
3.540	**0.0373**	**0.0462**	**0.0479**	**0.0285**	**0.0208**	0.0111	0.0103	–	0.0198	0.0186	0.0259
5.013	**0.0376**	**0.0465**	**0.0482**	**0.0289**	0.0211	0.0114	0.0106	0.0003	–	0.0193	0.0264
5.432	**0.0405**	**0.0494**	**0.0511**	**0.0317**	**0.0240**	0.0143	0.0135	0.0032	0.0029	–	0.0255
5.914	**0.0425**	**0.0514**	**0.0531**	**0.0337**	0.0260	0.0163	0.0155	0.0052	0.0049	0.0020	–

Table 2: Tukey-Kramer test results for the parameter α in non-targeted P105 micelles.

Power density, W/cm²	1.030	1.267	2.183	2.389	2.546	3.540	5.013	5.432	5.914
1.030	–	0.01472	0.01472	0.01472	0.01472	0.01472	0.01544	0.01472	0.01472
1.267	**0.01916**	–	0.01472	0.01472	0.01472	0.01472	0.01544	0.01472	0.01472
2.183	**0.02021**	0.00105	–	0.01472	0.01472	0.01472	0.01544	0.01472	0.01472
2.389	0.01021	0.00896	0.01001	–	0.01472	0.01472	0.01544	0.01472	0.01472
2.546	0.00340	**0.02256**	**0.02361**	0.01361	–	0.01472	0.01544	0.01472	0.01472
3.540	0.00472	**0.02389**	**0.02494**	**0.01493**	0.00132	–	0.01544	0.01472	0.01472
5.013	0.01126	**0.03042**	**0.03147**	**0.02147**	0.00786	0.00654	–	0.01544	0.01544
5.432	**0.01485**	**0.03401**	**0.03506**	**0.02505**	0.01145	0.01012	0.00359	–	0.01472
5.914	0.01282	**0.03198**	**0.03303**	**0.02303**	0.00942	0.00810	0.00156	0.00203	–

Table 3: Tukey-Kramer test results for the parameter β in F-P105 micelles.

Power density, W/cm²	1.009	1.062	1.030	1.267	2.183	2.389	2.546	3.540	5.013	5.432	5.914
1.009	–	1058	1165.5	1526	1321.5	1165.5	1206.4	1206.4	1257	1165.5	1706.1
1.062	503.4	–	1146.1	1511	1304.5	1146.1	1187.7	1187.7	1239.1	1146.1	1692.9
1.030	477.6	981	–	1588	1393	1245.9	1284.3	1284.3	1331.9	1245.9	1762
1.267	926.8	1430.2	449.2	–	1706.1	1588.2	1618.5	1618.5	1656.6	1588.2	2018.6
2.183	1045.4	**1548.8**	567.8	118.6	–	1393	1427.4	1427.4	1470.4	1393	1868.9
2.389	**2260.9**	**2764.3**	**1783.2**	1334	1215.5	–	1284.3	1284.3	1331.9	1245.9	1762
2.546	**2666.3**	**3170**	**2188.7**	**1740**	**1620.9**	405.5	–	1321.5	1367.9	1284.3	1789.3
3.540	**2444.1**	**2947.5**	**1966.5**	1517	1398.7	183.26	222.22	–	1367.9	1284.3	1789.3
5.013	**2521.3**	**3024.7**	**2043.7**	1595	**1475.9**	260.44	145.04	77.18	–	1331.9	1823.8
5.432	**2575.6**	**3079**	**2098**	**1649**	**1530.2**	314.76	90.72	131.5	54.32	–	1762
5.914	**2886.7**	**3390**	**2409**	1960	1841.2	625.8	220.31	442.5	365.4	311.03	–

micro-temperature might contribute to the release behavior, affecting the destruction parameter.

Figure 5 also shows that for power densities lower than 2 W/cm², α seems to be higher for P105 micelles, while for higher power densities the opposite pattern can be observed. A statistical analysis of the results revealed that the only significant differences are obtained for the lowest power density (1.03 W/cm²), with α being significantly higher ($p=0.03$) for non-targeted P105 micelles. For the highest power density (5.914 W/cm²), on the contrary, α is significantly lower ($p=4.42\times10^{-4}$) for F-P105 micelles, but this result must be considered carefully, as previously mentioned. At lower power densities, the presence of the folic acid moiety seems to for high power densities, when temperature may be a factor in the release mechanism, the presence of folic acid does not seem to play a role.

Table 4: Tukey-Kramer test results for the parameter β in non-targeted P105 micelles.

Power density, W/cm²	1.030	1.267	2.183	2.389	2.546	3.540	5.013	5.432	5.914
1.030	–	1609.39	1609.39	1609.39	1609.39	1609.39	1687.94	1609.39	1609.39
1.267	1134.4	–	1609.39	1609.39	1609.39	1609.39	1687.94	1609.39	1609.39
2.183	890.7	243.69	–	1609.39	1609.39	1609.39	1687.94	1609.39	1609.39
2.389	222.48	1356.8	1113.2	–	1609.39	1609.39	1687.94	1609.39	1609.39
2.546	265.39	869	625.3	487.9	–	1609.39	1687.94	1609.39	1609.39
3.540	309.15	1443.5	1199.8	86.66	574.5	–	1687.94	1609.39	1609.39
5.013	982.4	**2116.8**	**1873.1**	760	1247.8	673.3	–	1687.94	1687.94
5.432	1452.6	**2586.9**	**2343.3**	1230.1	**1718**	1143.4	470.1	–	1609.39
5.914	1323.4	**2457.8**	**2214.1**	1100.9	1588.8	1014.3	341	129.15	–

Table 5: Tukey-Kramer test results for the parameter λ in F-P105 micelles.

Power density, W/cm²	1.009	1.062	1.030	1.267	2.183	2.389	2.546	3.540	5.013	5.432	5.914
1.009	–	228.85	252.08	330.05	285.83	252.08	260.93	260.93	271.88	252.08	369.01
1.062	146.46	–	247.89	326.86	282.14	247.89	256.88	256.88	268.00	247.89	366.16
1.030	**314.53**	168.08	–	343.52	301.29	269.48	277.78	277.78	288.09	269.48	381.11
1.267	31.51	114.95	283.03	–	369.01	343.53	350.07	350.07	358.31	343.53	436.61
2.183	80.07	226.53	**394.60**	111.58	–	301.29	308.73	308.73	318.04	301.29	404.23
2.389	93.96	240.41	**408.50**	125.46	13.88	–	277.78	277.78	288.09	269.48	381.11
2.546	31.29	177.75	**345.80**	62.80	48.78	62.67	–	285.83	295.86	277.78	387.02
3.540	150.38	**296.84**	**464.90**	181.89	70.31	56.43	119.09	–	295.86	277.78	387.02
5.013	26.99	173.44	**341.50**	58.49	53.08	66.97	4.30	123.40	–	288.09	394.48
5.432	85.62	232.08	**400.20**	117.13	5.55	8.34	54.33	64.76	58.63	–	381.11
5.914	123.92	270.38	**438.50**	155.43	43.85	29.96	92.63	26.46	96.93	38.30	–

Table 6: Tukey-Kramer test results for the parameter λ in non-targeted P105 micelles.

Power density, W/cm²	1.030	1.267	2.183	2.389	2.546	3.540	5.013	5.432	5.914
1.030	–	284.56	284.56	284.56	284.56	284.56	298.45	284.56	284.56
1.267	176.99	–	284.56	284.56	284.56	284.56	298.45	284.56	284.56
2.183	282.40	105.40	–	284.56	284.56	284.56	298.45	284.56	284.56
2.389	159.75	17.25	122.65	–	284.56	284.56	298.45	284.56	284.56
2.546	9.78	186.77	**292.18**	169.53	–	284.56	298.45	284.56	284.56
3.540	11.79	188.79	**294.19**	171.54	2.01	–	298.45	284.56	284.56
5.013	16.12	160.88	266.28	143.63	25.90	27.91	–	298.45	298.45
5.432	89.67	87.32	192.72	70.07	99.45	101.47	73.56	–	284.56
5.914	**346.80**	169.81	64.41	187.06	**356.60**	**358.60**	**330.70**	257.13	–

Beta (β)

Beta is another temperature-dependent parameter, which is related to micelle reassembly (37). The model equations indicate that any increase in this parameter translates to an increase in the number of micelles (M) with time. This can be explained as follows: since most of the micelles are destroyed rapidly, the reassembly process increases proportionally. Furthermore, micelle destruction and reassembly happen simultaneously during insonation, until a pseudo-equilibrium is reached, when the number of micelles remains relatively constant over time (38).

The results obtained for the second parameter, β are shown in Table S2 (Supplementary Data) and in Figure 6, where the results are the average±standard deviation of the replicates indicated in Table S1 in the Appendix. The

Table 7: Comparison between parameters α, β and λ for P105 and F-P105 micelles.

Power density, W/cm²	α, μm⁻¹s⁻¹	β, μm³s⁻¹	λ, μms⁻¹
1.03	**0.0295**	0.4395	**0.0109**
1.267	0.0796	0.7154	**0.0198**
2.183	0.6473	**0.0147**	0.9606
2.389	0.4486	**0.0173**	0.6262
2.546	0.3383	0.3934	0.7488
3.54	0.9217	0.7850	0.3447
5.013	0.3895	0.5314	0.6167
5.432	0.2616	0.6008	0.7381
5.914	**0.0004**	**0.0020**	0.1161

The results are p-values obtained from a t-test. Significant results are shaded in gray (P105>F-P105) and blue (P105<F-P105).

results show a pattern of increase with increasing power density for this parameter, similar to the case of α. Since at lower power densities there are fewer cavitation events, there will be less microstreaming and lower incidences of shock waves, hence the amount of micelles destroyed is lower compared with that at higher power densities. Thus, re-assembly at lower intensities will also be lower. For targeted F-P105 micelles, the Tukey-Kramer test results are similar to the ones obtained for the α parameter, i.e. the differences observed between high and low power densities are significant (Table 3). This behavior is not as evident for P105 micelles, where β is only significantly higher for power densities equal or above 5.013 W/cm² (Table 4).

A comparison between F-P105 and P105 micelles revealed that β is significantly higher for non-targeted micelles at power densities of 2.183 W/cm² (p=0.015) and 2.389 W/cm² (p=0.017). Just like in the case of α, the β value at 5.914 W/cm² is significantly lower ($p=2.05\times10^{-3}$) for F-P105 micelles Again, for the reasons mentioned previously, this result must be considered carefully.

Lambda (λ)

Lambda is the drug encapsulation parameter, which is related to the rapid initial phase after insonation starts. This parameter is also temperature-dependent, and describes how quickly this initial phase of release ends, meaning that a long initial phase indicates a small value of λ and vice versa (37).

The results obtained for the third parameter (λ) are summarized in Table S2 (Supplementary Data) and in Figure 7, which shows results as average±standard deviation of the replicates indicated in Table S1 in Supplementary Data. The results do not show a clear pattern of λ with increasing power densities (Figure 7). Instead, λ values seem to fluctuate, probably indicating that this parameter is constant, for the power density range used in this study. The statistical analysis shown in Tables 5 and 6 confirm this observation: the values are not significantly different, except for a power density of 1.030 W/cm², when λ is significantly lower than any other power density, for F-P105 micelles. However, this result seems to be an outlier, since at the lower power densities (1.009, 1.062 and 1.030 W/cm²) the values of λ are constant and higher than the one at 1.030 W/cm², as are the values obtained at power densities equal or higher than 2.183 W/cm². Hence, for the range of power densities used in this study, λ does not seem to be correlated to the power density. The encapsulation rate depends on two mechanisms, encapsulation and diffusive rate (37), related to the fact that as micelles dissociate, their polymers possibly diffuse away. It was hypothesized that the higher the ultrasonic intensity, the higher the scatter of the polymers of the destroyed micelles (38). Thus, we would expect that, at higher power densities, the re-encapsulation process should take a longer period, with decreasing λ values.

The comparison between F-P105 and non-targeted P105 micelles shows that λ is significantly higher for P105, for the two lower power densities, 1.03 W/cm² (p=0.011) and 1.267 W/cm² (p=0.02). It is interesting to note that α is also significantly higher for P105, at the lowest power density, i.e. 1.03 W/cm². If micelles are quickly destroyed, then the end of the rapid phase will also be faster, with higher λ. This result suggests that non-targeted micelles are more sensitive to 70-kHz US, possibly due to a stabilizing role of the folate moiety, which may associate with more than one polymeric chain, thus strengthening the physical structure of the micelles. However, this was observed for the lower power density only. Studies with a range of lower power densities, up to 2 W/cm², would help test this hypothesis.

Conclusion

In this work, a DDS composed of Dox-encapsulating Pluronic® micelles (non-targeted or folate-targeted) as drug carriers and US as a trigger, was used to investigate the kinetics of acoustic release and subsequent re-encapsulation, when the insonation stops. For this purpose, a kinetic model (37, 38) was implemented in MATLAB and used to calculate three parameters related to the mechanism, α, β and λ. These parameters were studied as a function of power density for the two types of micelles, and the

statistical significance of the results was assessed using the Tukey-Kramer statistical test. Parameter α, which quantifies the rate of micellar destruction, and β, which measures the micelles' reassembly rate, were found to generally increase with increasing power densities. The parameter λ, which is related to the re-encapsulation of the drug in the micelles, did not change significantly with increasing power density, which suggests that the re-encapsulation is independent of the power densities used in this study.

A comparison between the results of folated and non-folated micelles was also conducted to examine the difference between both carriers. This comparison is critical as it signifies the difference in release behavior between two carriers that have the potential to be employed as DDS in vivo (32, 36, 42, 43). At lower power densities the parameters α and β for non-targeted micelles are significantly higher than for F-P105. This may indicate that the folated micelles are more stable than the non-targeted ones, for the reasons discussed previously. For power densities higher than 2.5 W/cm^2, there are no significant differences for any parameter, between F-P105 and P105. Possibly at these power densities, folate does not play a part in the structure stabilization. At the highest power density (5.914 W/cm^2) α and β are significantly higher for F-P105, but this result should be considered carefully since at this power density, other mechanisms such as hyperthermia and a change in micro viscosity may influence the drug release.

The modeling results obtained here are important in planning future experiments that may help understand the physical mechanism behind acoustically-triggered micellar drug delivery.

The fact that there are significant differences in the parameters obtained for folated and non-folated micelles at lower power densities, while no significant differences were observed for higher ones, suggest that further studies should use a lower range of power densities (up to 2.5 W/cm^2). Additionally, a larger number of replicates will increase the model robustness. Also to further refine this kinetic model, it will be important to automatically control several experimental parameters, such as the turning on and off of the US. The denoising process can also be improved using more accurate and specialized software, such as an automated wavelet processing software or other optimization methods. Furthermore, different models and optimization techniques (e.g. the Gauss-Newton method and Gradient descent algorithm) can be used and compared to the one described here, in order to achieve more accurate results. An optimized model will allow a better understanding of the mechanisms behind this DDS, which will contribute for the study and optimization of parameters used when the therapy is employed in a clinical setting.

Acknowledgments: The authors would like to acknowledge the funding from the American University of Sharjah Faculty Research Grant (FRG1-2012), Patient's Friends Committee-Sharjah, and Al Qasimi Foundation.

Conflict of interest statement: Authors state no conflict of interest. All authors have read the journal's publication ethics and publication malpractice statement available at the journal's website and hereby confirm that they comply with all its parts applicable to the present scientific work.

References

1. Jemal A, Bray F, Center MM, Ferlay J, Ward E, Forman D. Global cancer statistics. CA Cancer J Clin 2011;61:69–90.
2. Parkin DM, Bray F, Ferlay J, Pisani P. Global cancer statistics, 2002. CA Cancer J Clin 2005;55:74–108.
3. Kundu B, Ghosh D, Sinha MK, Sen PS, Balla VK, Das N, et al. Doxorubicin-intercalated nano-hydroxyapatite drug-delivery system for liver cancer: an animal model. Ceram Int 2013;39:9557–66.
4. Gandhi H, Patel VB, Mistry N, Patni N, Nandania J, Balaraman R. Doxorubicin mediated cardiotoxicity in rats: Protective role of felodipine on cardiac indices. Environ Toxicol Pharmacol 2013;36:787–95.
5. Cuomo F, Mosca M, Murgia S, Avino P, Ceglie A, Lopez F. Evidence for the role of hydrophobic forces on the interactions of nucleotide-monophosphates with cationic liposomes. J Colloid Interface Sci 2013;410:146–51.
6. Jhaveri AM, Torchilin VP. Multifunctional polymeric micelles for delivery of drugs and siRNA. Front Pharmacol 2014;5:77.
7. Jones M, Leroux J. Polymeric micelles – a new generation of colloidal drug carriers. Eur J Pharm Biopharm 1999;48:101–11.
8. Torchilin VP. Micellar nanocarriers: pharmaceutical perspectives. Pharm Res 2007;24:1–16.
9. Blanco E, Kessinger CW, Sumer BD, Gao J. Multifunctional micellar nanomedicine for cancer therapy. Exp Biol Med (Maywood) 2009;234:123–31.
10. Alexandridis P, Alan Hatton T. Poly(ethylene oxide) – poly(propylene oxide) – poly(ethylene oxide) block copolymer surfactants in aqueous solutions and at interfaces: thermodynamics, structure, dynamics, and modeling. Colloids Surface A: Physicochemical and Engineering Aspects 1995;96:1–46.
11. Kabanov AV, Alakhov VY. Pluronic block copolymers in drug delivery: from micellar nanocontainers to biological response modifiers. Crit Rev Ther Drug Carrier Syst 2002;19:1–72.
12. Kabanov AV, Batrakova EV, Melik-Nubarov NS, Fedoseev NA, Dorodnich TY, Alakhov VY, et al. A new class of drug carriers: micelles of poly(oxyethylene)-poly(oxypropylene) block copolymers as microcontainers for targeting drugs from blood to brain. J Control Release 1992; 22:141–58.
13. Kabanov AV, Nazarova IR, Astafieva IV, Batrakova EV, Alakhov VY, Yaroslavov AA, et al. Micelle formation and solubilization of fluorescent probes in poly(oxyethylene-b-oxypropylene-b-oxyethylene) solutions. Macromolecules 1995;28:2303–14.

14. Rapoport NY, Christensen DA, Fain HD, Barrows L, Gao Z. Ultrasound-triggered drug targeting of tumors in vitro and in vivo. Ultrasonics 2004;42:943–50.
15. Husseini GA, Pitt WG. Ultrasonic-activated micellar drug delivery for cancer treatment. J Pharm Sci 2009;98:795–811.
16. Husseini GA, Pitt WG. Micelles and nanoparticles for ultrasonic drug and gene delivery. Adv Drug Deliv Rev 2008;60:1137–52.
17. Adams ML, Lavasanifar A, Kwon GS. Amphiphilic block copolymers for drug delivery. J Pharm Sci 2003;92:1343–55.
18. Maeda H. The enhanced permeability and retention (EPR) effect in tumor vasculature: the key role of tumor-selective macromolecular drug targeting. Adv Enzyme Regul 2001;41:189–207.
19. Husseini GA, Pitt WG. The use of ultrasound and micelles in cancer treatment. J Nanosci Nanotechnol 2008;8:2205–15.
20. Kabanov AV, Batrakova EV, Alakhov VY. Pluronic block copolymers for overcoming drug resistance in cancer. Adv Drug Deliv Rev 2002;54:759–79.
21. Husseini GA, Christensen DA, Rapoport NY, Pitt WG. Ultrasonic release of doxorubicin from Pluronic P105 micelles stabilized with an interpenetrating network of N,N-diethylacrylamide. J Control Release 2002;83:303–5.
22. Gaucher G, Dufresne MH, Sant VP, Kang N, Maysinger D, Leroux JC. Block copolymer micelles: preparation, characterization and application in drug delivery. J Control Release 2005;109:169–88.
23. Torchilin V. Multifunctional and stimuli-sensitive pharmaceutical nanocarriers. Eur J Pharm Biopharm 2009;71:431–44.
24. Yu MK, Park J, Jon S. Targeting strategies for multifunctional nanoparticles in cancer imaging and therapy. Theranostics 2012;2:3–44.
25. Byrne JD, Betancourt T, Brannon-Peppas L. Active targeting schemes for nanoparticle systems in cancer therapeutics. Adv Drug Deliv Rev 2008;60:1615–26.
26. Sethuraman VA, Bae YH. TAT peptide-based micelle system for potential active targeting of anti-cancer agents to acidic solid tumors. J Control Release 2007;118:216–24.
27. Hilgenbrink AR, Low PS. Folate receptor-mediated drug targeting: from therapeutics to diagnostics. J Pharm Sci 2005;94:2135–46.
28. Leamon CP, Reddy JA. Folate-targeted chemotherapy. Adv Drug Deliv Rev 2004;56:1127–41.
29. Shen Z, Li Y, Kohama K, Oneill B, Bi J. Improved drug targeting of cancer cells by utilizing actively targetable folic acid-conjugated albumin nanospheres. Pharmacol Res 2011;63:51–8.
30. Sudimack J, Lee RJ. Targeted drug delivery via the folate receptor. Adv Drug Deliv Rev 2000;41:147–62.
31. Zhao X, Li H, Lee RJ. Targeted drug delivery via folate receptors. Expert Opin Drug Deliv 2008;5:309–19.
32. Yoo HS, Park TG. Folate receptor targeted biodegradable polymeric doxorubicin micelles. J Control Release 2004;96:273–83.
33. Hayama A, Yamamoto T, Yokoyama M, Kawano K, Hattori Y, Maitani Y. Polymeric micelles modified by folate-PEG-lipid for targeted drug delivery to cancer cells in vitro. J Nanosci Nanotechnol 2008;8:3085–90.
34. Husseini GA, Pitt WG, Martins AM. Ultrasonically triggered drug delivery: breaking the barrier. Colloids Surf B Biointerfaces 2014;123C:364–86.
35. Husseini GA, Velluto D, Kherbeck L, Pitt WG, Hubbell JA, Christensen DA. Investigating the acoustic release of doxorubicin from targeted micelles. Colloids Surf, B 2013;101:153–5.
36. Kim D, Gao ZG, Lee ES, Bae YH. In vivo evaluation of doxorubicin-loaded polymeric micelles targeting folate receptors and early endosomal pH in drug-resistant ovarian cancer. Mol Pharm 2009;6:1353–62.
37. Husseini GA, Stevenson-Abouelnasr D, Pitt WG, Assaleh KT, Farahat LO, Fahadi J. Kinetics and Thermodynamics of Acoustic Release of Doxorubicin from Non-stabilized polymeric Micelles. Colloids Surf, A 2010;359:18–24.
38. Stevenson-Abouelnasr D, Husseini GA, Pitt WG. Further investigation of the mechanism of Doxorubicin release from P105 micelles using kinetic models. Colloids Surf, B 2007;55:59–66.
39. Husseini GA, Myrup GD, Pitt WG, Christensen DA, Rapoport NY. Factors affecting acoustically triggered release of drugs from polymeric micelles. J Control Release 2000;69:43–52.
40. Haynes W. Tukey's range test. In: Dubitzky W, Wolkenhauer O, Cho K-H, Yokota H, editors. Encyclopedia of systems biology. New York: Springer, 2013:2303–2304.
41. Kramer CYC. Extension of multiple range tests to group means with unequal numbers of replications. Biometrics 1956;12:307–10.
42. Staples BJ, Pitt WG, Roeder BL, Husseini GA, Rajeev D, Schaalje GB. Distribution of doxorubicin in rats undergoing ultrasonic drug delivery. J Pharm Sci 2010;99:3122–31.
43. Staples BJ, Roeder BL, Pitt WG. Quantification of doxorubicin concentration in rat tissues using polymeric micelles in ultrasonic-drug delivery. In: Annual Meeting of the Society for Biomaterials; 2006. Pittsburgh, PA, USA, 2006:476.

Supplemental Material: The online version of this article (DOI: 10.1515/ejnm-2015-0045) offers supplementary material, available to authorized users.

Bionotes

Ana M. Martins
Department of Chemical Engineering, American University of Sharjah, Sharjah, UAE

Ana M. Martins is a research scientist at the Ultrasound in Cancer Research Group at American University of Sharjah. She obtained her BSc in Biochemistry and her PhD in Biochemistry/Enzymology from the University of Lisbon (Portugal). Dr. Martins has a wide research experience: after completing her PhD she spent 7 years at Virginia Polytechnic Institute and State University, first in Virginia Bioinformatics Institute, later in the Department of Biological Sciences. Dr. Martins has a systems biology approach to research, combining experimental and modeling work to understand the function of biochemical systems. Her current research interests include the development of drug delivery systems using liposomes and ultrasound as a trigger.

Rafeeq Tanbour
Department of Chemical Engineering, American University of Sharjah, Sharjah, UAE

Rafeeq Tanbour graduated in 2012 with a BSc degree in Chemical Engineering from An-Najah National University in Nablus, Palestine. Then he moved to the United Arab Emirates in 2013 and began a MSc program in Chemical Engineering at the American University of Sharjah (AUS), and graduated in January, 2015. During his MSc studies, he focused on the use of drug delivery systems as possible cancer therapy, in particular how ultrasound can be utilized as a trigger to release drugs from polymeric micelles. He is also a member of the Ultrasound in Cancer Research Group at AUS and Jordanian Engineering Association.

Mohammed A. Elkhodiry
Department of Chemical Engineering, American University of Sharjah, Sharjah, UAE

Mohammed A. Elkhodiry is a Researcher in the American University of Sharjah's Ultrasound in Cancer Research Group and a senior undergraduate Chemical and Biomedical Engineering student at the same university. His current research areas are drug delivery for chemotherapeutic treatment and regenerative liver tissue engineering. His work focuses on synthesizing protein-modified liposomal nanocarriers for targeting cancer. He is the Chairman and co-founder of the IEEE Engineering in Medicine and Biology Society (EMBS) Student Chapter at AUS.

Ghaleb A. Husseini
Department of Chemical Engineering, American University of Sharjah, PO Box 26666, Sharjah, UAE
ghusseini@aus.edu

Ghaleb A. Husseini (BSc 1995–MSc 1997–PhD 2001) graduated with a PhD in Chemical Engineering (Biomedical Engineering emphasis) from Brigham Young University in 2001 and joined the American University of Sharjah as an Assistant Professor in the Chemical Engineering Department in 2004. He was promoted to Associate Professor and Professor in 2008 and 2013, respectively. Dr. Husseini works in the area of ultrasound-activated drug delivery. His research involves sequestering chemotherapeutic agents in liposomes, micelles and other nanoparticles, and studying their controlled release triggered by ultrasound. Dr. Husseini has recently established the Ultrasound in Cancer Research Group at AUS using an internal grant. He has published 78 journal articles (in addition to one book chapter and one patent) and 42 conference papers/abstracts. He has been elected into the Distinguished Lecturer Program-IEEE-EMBS (Jan 2014–Dec 2015).